Publications of the Astronomical Society of the Pacific
106: 327–336, 1994 March

Astrometry with *Hubble Space Telescope* Fine Guidance Sensor Number 3: Position-Mode Stability and Precision[1]

G. F. BENEDICT, B. MCARTHUR, E. NELAN, D. STORY, AND A. L. WHIPPLE

McDonald Observatory, University of Texas, Austin, Texas 78712
Electronic mail: fritz@dorrit.as.utexas.edu, mca@clyde.as.utexas.edu, nelan@scivax.stsci.edu, story@scivax.stsci.edu, alw@astro.as.utexas.edu

W. H. JEFFERYS AND Q. WANG

Astronomy Department, University of Texas, Austin, Texas 78712
Electronic mail: bill@clyde.as.utexas.edu, wang@astro.as.utexas.edu

P. J. SHELUS, P. D. HEMENWAY, AND J. MCCARTNEY

McDonald Observatory, University of Texas, Austin, Texas 78712
Electronic mail: pjs@astro.as.utexas.edu, paul@astro.as.utexas.edu, james@astro.as.utexas.edu

WM. F. VAN ALTENA

Yale University, P. O. Box 6666, New Haven, Connecticut 06511
Electronic mail: vanalten@astro0.astro.yale.edu

R. DUNCOMBE

Aerospace Engineering Department, University of Texas, Austin, Texas 78712
Electronic mail: duncombe@utcsr.ae.utexas.edu

O. G. FRANZ

Lowell Observatory, Mars Hill Road, 1400 West, Flagstaff, Arizona 86001
Electronic mail: ogf@lowell.edu

L. W. FREDRICK

University of Virginia, Charlottesville, Virginia 22903
Electronic mail: lwf@astsun.astro.virginia.edu

Received 1993 November 4; accepted 1993 December 21

ABSTRACT. We report results from a test exploring the long- and short-term astrometric stability of *Hubble Space Telescope* Fine Guidance Sensor #3. A test field was observed 40 times over 522 days to determine the precision and accuracy of FGS astrometry and to measure the character and magnitude of possible secular scale changes. We examine the astrometric data and the associated guide-star data to determine random errors. These data are also explored to find sources of systematic error. After correcting for some systematic effects we obtain a precision of 0.002 arcsec (2 mas) per observation (RSS of x and y). This is relative astrometry within a central 2.5 arcmin FGS field of view for any orientation. We find that the scale varies over time and confirm the sense of the trend with independent data. From the 40 observation sets we produce a catalog of an astrometry test field containing eight stars whose relative positions are known to an average 0.7 and 0.9 mas in x and y. One reference star has a relative parallax of 3.1 ± 0.5 mas. Finally, we report that eleven observation sets acquired over 387 days produce parallaxes and relative positions with 1-mas precision.

1. INTRODUCTION

Since the selection of the fine guidance sensors (FGSs) as the guiding devices aboard *Hubble Space Telescope (HST)* in the mid 1970's (Wissenger and Carricato 1976), it has been asserted that astrometry with RSS precision approaching 3 mas would be possible (e.g., Jefferys et al. 1985). We have previously detailed (Benedict et al. 1992) why we chose FGS 3 to be the astrometer. For those unfamiliar with FGS astrometry data Benedict et al. (1992) and Bradley et al. (1991) provide useful background. The calibration of the FGS 3 optical field angle distortion (OFAD) will be discussed in a subsequent paper (Jefferys et al. 1994). This paper deals with POS mode astrometry. TRANS mode astrometry, involving the detailed analysis of the interferometer response function (in particular for double stars), will be discussed in a separate paper.

The pre-launch estimate of the single-observation astrometric precision of *HST* was 2.7 mas, as an RSS of the x and y axis precisions (Bahcall and O'Dell 1979). We now

[1]Based on observations with the NASA/ESA *Hubble Space Telescope*, obtained at the Space Telescope Science Institute, which is operated by the Association of Universities for Research in Astronomy, Inc., under NASA contract NAS5-26555.

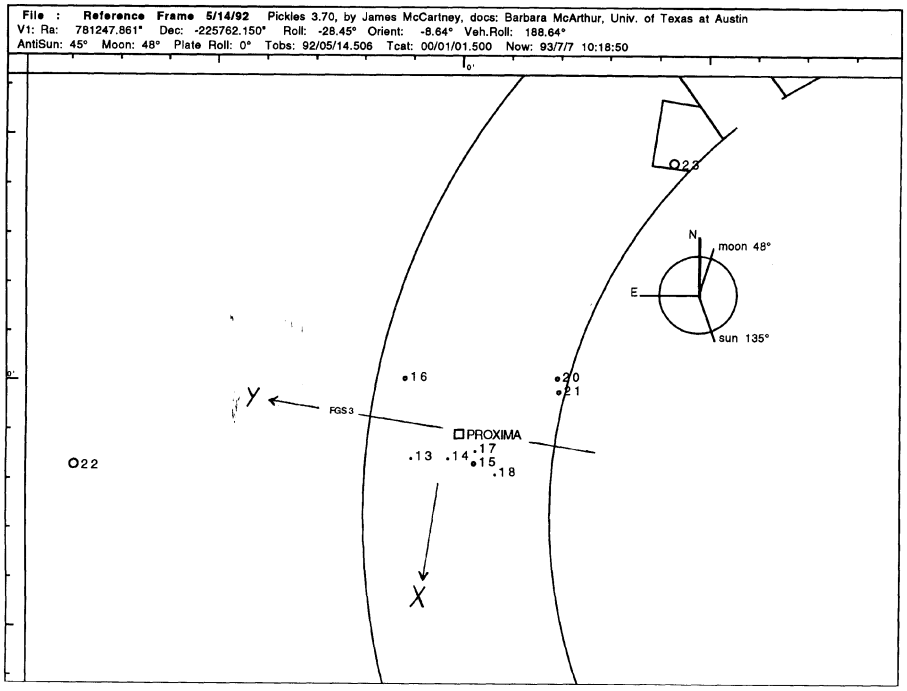

FIG. 1—*HST* orientation for observation set 6 (Table 1). On this day, the *HST* roll was off-nominal by −28°.5. The FGS 3 instrumental x and y axes are shown. Star ID numbers are from Table 2.

present evidence that this goal for FGS astrometry has been met for the central 2.5 arcmin of FGS 3.

A test field was observed 40 times over 522 days to determine the precision of FGS astrometry and to measure the character and magnitude of possible secular scale changes. Observations started on 1992 March 23 20:35:30 UT. The first 23 observation sets were acquired as part of the *HST* Astrometry Science Team Science Verification campaign. Since the field contains a scientifically interesting target, Proxima Centauri, monitoring continued past Science Verification. We continue to monitor Proxima Centauri to search for astrometric evidence of companions. We feel that it is important to communicate the attained precision of FGS astrometry to the astronomical community prior to the end of the monitoring program. To this end we present astrometry of the Proxima Centauri reference frame. These data include observations sets from the Science Verification test and from the planet monitoring. We will illustrate the long- and short-term astrometric stability of FGS 3 and discuss the astrometric precision. Results of the companion search and a discussion of the accuracy of FGS astrometry will be presented at the conclusion of the monitoring.

2. THE DATA

In the following discussion an *observation* consists of data acquired for a single star. An *observation set* includes all data for all stars observed during one orbit. Such a set is built up by moving the FGS 3 instantaneous field of view (a square 5×5 arcsec) from star to star within the total FGS 3 field of view (the pickle-shaped region outlined in Fig. 1) during the orbit.

Most of the observation sets discussed below were acquired in less than 25 min. The order of observation is the check star (Proxima Centauri) those reference stars 13 through 23 located within the FGS 3 pickle, then return to the check star. For the observation set acquired 1992 May 14 shown in Fig. 1, we did not observe reference stars 21, 22, and 23. The latter star was in the field of view of the FGS 3 optical control wave front sensor, a region unavailable for FGS 3 observations. Star 21 was too close to the edge of the pickle to observe.

2.1 Temporal and Spatial Distribution

We attempted 47 observation sets from 1992 March 23 to 1993 June 25. For the rest of this paper dates will be given as Julian Day–2448000, hereafter referred to as *day*. Columns 1 and 2 in Table 1 provide a convenient mapping between day and calendar data for the 40 successful observation sets.

In six of the lost observation sets loss of lock occurred, caused by vibrations of *HST* (induced by solar array flexure due to day-to-night transitions). Only one set was lost because of an *HST* safing event. Our astrometry loss-of-lock statistics are similar to other science instruments. However, instead of degrading our results, we lose the entire observation set. *HST* cannot recover from loss of lock while doing astrometry. A new recentering algorithm was installed in the *HST* Pointing Control System in January 1993. We have incurred no losses of lock since.

TABLE 1
Stability Summary

JD -	1992				Jitter Balls for all Stars			S/C Environ.		Guide Stars							Check Star Closure Differences				1992
2448000.0	day	set	N*	NS	<sx>	<sy>	<RSS>	d/n/t	roll	DGS	m1	m2	dx1	dy1	dx2	dy2	dx ±		dy ±		day
705.358	83	1	5	5	2.2	3.1	3.7	d	o-n (+)	2	11.4	11.4	-3.7	2.1	0.2	0.1	**-5.9**	**2.6**	-3.2	3.9	83
714.3249	92	2	6	5	2.4	**4.0**	**4.6**	n	o-n (+)	2	11.4	11.4	0.6	-1.1	-0.2	-1.0	-0.8	3.2	-1.1	7.4	92
724.308	102	3	6	6	2.2	**4.4**	**5.0**	n	o-n (+)	1	11.4	11.4	0.7	-0.7	-1.9	-0.5	-4.0	5.2	-1.1	14.9	102
736.897	115	4	6	6	1.9	2.7	3.3	n	n	2	11.4	11.4	0.2	-1.4	-0.1	-0.9	-3.0	3.2	-3.6	5.3	115
751.89	130	5	6	6	1.6	2.1	2.7	d	o-n (-)	2	11.4	11.4	0.0	2.5	0.0	0.2	-1.1	2.6	-1.8	3.2	130
757.009	135	6	7	**6**	2.3	3.0	3.7	n	o-n (-)	2	11.4	11.4	0.4	-0.6	-0.2	-0.7	-5.5	6.1	-3.0	8.8	135
760.361	138	7	6	6	2.7	2.4	3.6	n	o-n (+)	1	10.9	11.6	-0.7	0.2	**-4.7**	-3.3	4.3	2.7	-3.8	3.3	138
770.208	148	8	5	**4**	2.2	2.5	3.3	n	o-n (+)	1	10.9	11.6	-0.2	-0.3	-3.0	-1.7	0.6	2.6	-4.5	4.3	148
784.202	162	9	6	6	1.9	2.9	3.5	n	o-n (+)	1	10.9	11.6	0.5	-0.5	-0.9	0.1	**-6.0**	**2.7**	-4.4	4.5	162
790.63	169	10	5	5	2.1	3.0	3.7	t	n	1	10.9	11.6	0.3	0.3	0.2	-0.3	**-7.5**	**2.8**	-5.1	4.4	169
814.162	192	11	9	**8**	3.3	2.5	**4.1**	n	o-n (+)	1	9.9	12.4	0.3	0.3	0.0	-0.4	**9.1**	**5.7**	-2.7	3.8	192
814.224	192	12	8	8	2.2	2.6	3.4	n	o-n (+)	1	9.9	12.4	-0.2	0.7	-0.1	-2.2	**8.8**	**3.7**	-2.9	3.3	192
819.921	198	13	7	7	1.8	2.4	3.0	n	n	2	9.9	9.5	1.7	**-4.6**	-0.2	-0.5	-2.2	2.8	-2.5	4.8	198
823.871	202	14	10	10	2.0	2.8	3.4	n	o-n (+)	1	9.9	12.4	0.5	-0.1	-2.3	**-4.9**	**6.2**	**3.1**	-2.9	3.5	202
823.933	202	15	10	10	2.1	2.9	3.6	t	o-n (+)	1	9.9	12.4	0.5	-0.5	-2.3	**-5.6**	2.7	3.1	-3.4	4.3	202
828.022	206	16	6	6	1.9	2.2	2.9	n	n	2	9.9	9.5	1.2	-0.5	-0.7	0.6	**-5.9**	**2.7**	-2.8	3.3	206
831.029	209	17	10	10	2.1	3.1	3.7	d	o-n (+)	1	9.9	12.4	0.8	-0.3	-0.8	**-5.0**	3.2	3.3	-4.3	5.7	209
845.697	224	18	10	**9**	2.3	3.4	**4.1**	d	n	1	9.9	12.4	-1.0	0.8	0.9	3.1	0.3	3.1	0.5	5.6	224
845.759	224	19	10	10	2.2	2.6	3.4	d	n	1	9.9	12.4	-0.7	-0.9	2.2	3.8	4.0	4.0	-2.0	4.5	224
845.831	224	20	8	8	2.0	2.7	3.3	d	n	1	9.9	11.5	0.9	0.5	-1.7	-2.6	2.6	3.8	-0.6	7.4	224
856.475	234	21	8	8	2.2	2.2	3.1	d	n	2	11.6	10.8	2.2	-0.1	0.1	-0.2	-0.2	3.3	2.2	4.0	234
858.344	236	22	10	**9**	2.0	2.7	3.3	d	o-n (-)	1	9.9	12.4	1.0	0.4	0.6	0.8	-4.2	3.4	-0.3	4.4	236
859.214	237	23	10	**9**	**4.9**	3.6	**6.1**	d	o-n (-)	1	9.9	12.4	0.7	0.1	-0.9	-1.3	-2.3	3.6	0.3	4.1	237
867.321	245	24	8	**7**	3.9	3.1	**5.0**	d	n	1	11.2	12.4	0.9	0.6	0.1	2.1	-4.0	3.8	-0.3	4.1	245
886.634	265	25	8	8	**8.8**	3.3	**9.4**	d	n	2	12.4	10.8	0.2	-2.7	-0.5	0.3	2.2	3.9	0.4	4.8	265
897.479	275	26	8	**7**	4.2	2.9	**5.1**	d	n	2	11	10.6	2.5	-3.9	0.3	0.4	-2.3	3.3	3.0	3.5	275
906.592	285	27	8	8	4.4	3.3	**5.5**	d	n	2	11	10.6	1.6	1.3	0.3	1.0	-1.8	4.0	-0.9	4.1	285
978.033	356	28	4	4	4.3	3.1	**5.3**	t	n	1	10.7	10.9									356

JD -	1993				Jitter Balls for all Stars			S/C Environ.		Guide Stars							Check Star Closure Differences				1993
2448000.0	day	set	N*	NS	<sx>	<sy>	<RSS>	d/n	roll	DGS	m1	m2	dx1	dy1	dx2	dy2	dx ±		dy ±		day
988.777	1	29	8	**7**	**5.0**	**5.9**	**7.7**	d	n	1	10.8	11	0.2	0.4	1.6	-0.7	-1.0	3.7	-0.1	5.1	1
999.618	12	30	7	**4**	**5.5**	**6.4**	**8.4**	d	n	2	11.7	9.6	-0.3	1.8	-0.6	-0.4	2.4	3.7	-4.0	5.7	12
1009.402	21	31	8	8	**5.4**	**5.8**	**7.9**	d	n	2	11.9	9.5	0.1	-1.2	0.1	0.0	-4.3	107.5	-1.1	60.8	21
1092.500	104	32	8	**6**	4.3	**5.7**	**7.1**	t	n	1	11.6						-4.4	3.4	-2.0	5.5	104
1105.475	117	33	8	8	4.1	**5.9**	**7.2**	t	n	1	11.6						**6.7**	**3.4**	**-21.0**	**5.3**	117
1116.186	128	34	7	**6**	4.6	**5.9**	**7.4**	n	n	1	11.4						2.3	3.0	-4.0	3.9	128
1127.088	139	35	6	6	4.7	**6.4**	**8.0**	t	n	1	11.4						**-8.4**	**3.1**	-4.0	3.7	139
1136.855	149	36	6	6	4.2	**5.7**	**7.1**	d	n	1	11.1						**-18.4**	**3.3**	-1.0	4.8	149
1155.221	167	37	6	**5**	4.2	**5.7**	**7.1**	n	n	1	11.1						**9.8**	**3.3**	-3.6	4.0	167
1164.252	176	38	6	**5**	4.1	**5.3**	**6.6**	n	n	1	11.1						**9.8**	**3.3**	-3.6	6.0	176
1211.251	223	39	8	**7**	4.9	**7.0**	**8.5**	n	n	1	11.4						-0.7	3.8	-4.6	4.1	223
1227.723	240	40	8	**7**	4.2	**5.5**	**7.0**	t	n	1	11.4						**-12.4**	**3.3**	-4.0	4.0	240

There are two obvious gaps in our monitoring of this field. Centered at day 845, the first gap occurred because *HST* is restricted from observing objects closer than 50° from the Sun. The second gap (day 1050) was caused by a combination of guide-star unavailability and equipment problems. FGS 2 was removed from guiding service on day 1030. After determining that guiding with a single FGS was a viable operational mode, the nominal *HST* scheduling lag of around ten weeks resulted in this second gap.

Figure 1 presents a finding chart of our test field. The orientation is off-nominal, showing our commanded attitude for day 757. Stars 22 and 23, well outside the FGS 3 field of view, were only observed during eight observation sets from day 814 through day 859. These are the sets with nine or more stars (N^*) in Table 1. All sets containing stars 22 and 23 were observed with but a single orientation.

Table 2 lists magnitudes and colors of the stars in our test field. Photometric data for stars 22 and 23 are from the Guide Star Selection System catalog, which contains no color information.

2.2 The Error Budget for *HST* FGS Astrometry

Our goal is to obtain as precise relative position measurements as possible within the FGS 3 pickle. Many factors determine the ultimate astrometric precision. These can be within the FGS or outside factors associated with the *HST*. Other factors are associated with the orbital environment.

Short-term components are those which occur on time scales of minutes and affect a single observation or observation set. The major short-term contributor is the *HST*

jitter. This is telescope motion caused primarily by solar array motions driven by orbital day/night cycles. Less important are the responses to actuator motions, such as filter wheels and high-gain antennae. There are also several possible thermal stimuli, including changes within FGS 3 caused by temperature variations and temperature-induced changes in secondary mirror position, the so-called secondary mirror breathing (Ftaclas 1993). A short-term factor associated with orbital environment is the South Atlantic Anomaly. This is likely not an important factor, since automatic scheduling prohibits observing during passage through the most intense sections.

The final factors we shall consider to have an effect on each observation and every observation set are the optical field angle distortion (OFAD) and lateral color. OFAD is partially defined as whatever distortions remain after optical effects caused by ripples and other figuring imperfections in the asphere and pickoff mirrors within FGS 3 (Bradley et al. 1991) are removed in our preprocessing. It also includes uncorrected primary–secondary optical aberration. If not properly mapped, all relative positions will be degraded when comparing observation sets acquired with different roll orientations. Details of our OFAD mapping will be provided elsewhere (Jefferys et al. 1994). We simply state that OFAD contributes less than 0.001 arcsec per axis to the astrometry error budget in the pickle center.

Lateral color is another possible problem that would result in degraded positions when comparing observation sets acquired with different roll orientations. Each FGS contains refractive elements. Relative positions of stars within FGS 3 may depend on the color of the observed stars and the position angle of the radius vector between the two stars within FGS 3. Large color differences ($\Delta B - V \sim 2$) could cause up to 1.5 mas positional shifts for stars located in the center of the pickle. These shifts would be primarily along the long axis of FGS 3 (Abramowicz-Reed 1993). FGS photomultiplier tube (Bradley et al. 1991) mismatch might also contribute to this problem.

Long-term contributors to the FGS 3 error budget include changes in *HST* plate scale caused by desorption of the graphite epoxy metering truss (Benedict et al. 1992). The scale is the linear term in our OFAD. Hence, OFAD is a long- and a short-term factor. Since the primary–secondary mirror separation is changing (Hasan et al. 1993), and since graphite epoxy holds many FGS optical components in alignment, we might expect to see long-term changes within FGS 3.

2.3 Systematic Effects and Random Errors

We shall explore random errors and systematic effects first using Table 1, our master stability summary. The columns contain JD–2448000 and day of year (day); a running set number (set); the number of stars observed (N^*), the number of stars entering into the plate solution (NS) (described in Sec. 3.1); the average jitter ball dimensions in x and y, and the RSS of x and y (see Benedict et al. 1992 for definition and examples). Observation sets with average dispersions greater than 4 mas are displayed in boldface. We next list information about the spacecraft environment. Observation sets were acquired during spacecraft day (d), or night (n), or terminator crossing (t). *HST* roll was either nominal (n) or off-nominal (o-n) with the sun shining on FGS 1 ($-$) or FGS 3 ($+$). Guide star data includes an identifier of the dominant guide star (DGS); guide star magnitudes from the Guide Star Selection System catalog ($m1$ and $m2$); and amount of guide star drift during the observation set ($dx1,2$ and $dy1,2$). Drifts larger than 4 mas are shown in boldface. Finally we list the check star drift (dx and dy) and associated errors during an observation set. Those drifts greater than 4 mas with significance greater than two standard deviations are boldface. Lastly, we repeat the day number as an aid to navigation.

Guide-star jitter, which includes solar-array-induced vehicle motions, and observation noise contribute to our random error. Each observation consists of over 2400 measures of the position of a star. The standard deviation of these measures in x and in y defines a characteristic jitter ball size. For a more detailed explanation and a plot of a representative jitter ball, see Benedict et al. (1992), Fig. 11. The average jitter ball size per observation set is given in Table 1 ($\langle sx \rangle$ and $\langle sy \rangle$).

Inspecting Table 1 for obvious systematic trends that may be contributing to the observed instabilities, we see that the jitter balls have increased dramatically for day 859

TABLE 2
Photometry and Relative Positions of Reference Frame Stars

Star ID	V		B-V		ξ † (arcsec)		η (arcsec)		RA †† (degrees)	DEC (degrees)
13	15.10	± 0.07	0.72	± 0.10	38.6747	± 0.0008	54.1021	± 0.0010	217.481909	-62.689236
14	15.76	0.06	0.87	0.17	31.6974	0.0006	9.5335	0.0008	217.454596	-62.689342
15	14.36	0.11	0.66	0.14	33.5916	0.0006	-22.9465	0.0008	217.435381	-62.691332
16	14.58	0.09	0.52	0.12	-55.7182	0.0009	76.6803	0.0011	217.486078	-62.662344
17	15.32	0.08	0.73	0.12	17.4660	0.0006	-21.8306	0.0007	217.434456	-62.686862
18	15.14	0.05	1.53	0.07	41.9904	0.0007	-49.4220	0.0010	217.420395	-62.694833
20	14.30	0.11	1.05	0.15	-84.7881	0.0006	-107.9642	0.0009	217.372909	-62.662739
21	14.43	0.09	0.69	0.13	-68.4853	0.0007	-111.3983	0.0010	217.372467	-62.667362
22	11.83	0.6	-	-	111.7940	0.0033	460.2490	0.0040	217.731744	-62.690881
23	11.19	0.6	-	-	-365.7880	0.0028	-205.6991	0.0036	217.286787	-62.590154

† Day 757 orientation, OFAD scale
†† Positions are derived by rotating ξ, η by R =1.40703 radians, and applying offsets from star 15 (see text)

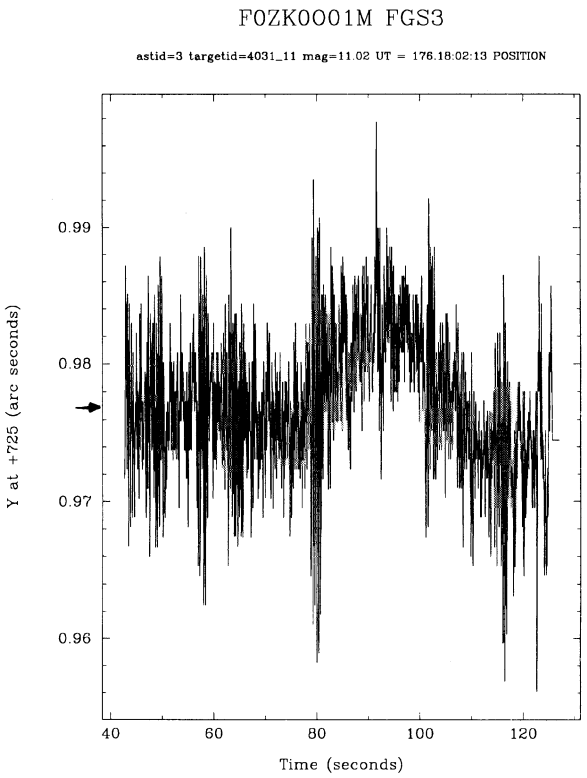

FIG. 2—An example of median filtering. The y position as a function of time during the first check star observation on day 1164 (set 38). Note the large transient vehicle disturbances at $t=80$ s and the systematic displacement during $90<t<110$ s. The position (725.9767 arcsec) determined by the median filter is marked by the arrow on the y axis.

and after. On this date new fine error signal gain K factors (K_1, see Bradley et al. 1991 for details) were adopted in the onboard processing. Until day 859 we only observed stars in the center of the pickle. Recall that the interferometer response function changes with location in FGS 3 [Benedict et al. 1992, Fig. 5(a)]. Larger gains were necessary to obtain valid positions throughout the pickle. But larger gains exaggerate random fluctuations in position. The average jitter ball RSS size is 3.6 mas pre-day 859 and 6.9 mas after. The hope is that while the jitter balls are larger, the precision of the resulting position is little affected, since we make over 2400 measurements per observation. The residuals discussed in Sec. 3.2 indicate slight degradation.

We have implemented several methods to minimize the impact of these jitter-related random and predominantly short-term contributors to the error budget. First, we determine our positions from the median of the data, not the mean. The median is a more robust estimator for data with a strong central tendency, especially for data containing outliers (Press et al. 1992, Ch. 14.2). Figure 2 shows the y position as a function of time for the first check star in observation set 38. This day the spacecraft was not a particularly stable platform at the millisecond of arc level. The excursion centered at time 92 s was a major contributor to the larger than average uncertainty in drift for Y (the set 38 Closure Star *dy* in Table 1). The position determined by the median filter is indicated by the arrow on the Y axis.

In extreme cases we could resort to selective data editing. For example, a position derived from data acquired between 42 and 78 s in Fig. 2 might be "better." However, none of the data for this paper have been selectively edited.

An additional solution to *HST* jitter is to replace the existing solar arrays with arrays designed to be far less excited by terminator crossing. This is expected to occur during the first servicing mission, scheduled for December 1993.

The other obvious trends are in the check star drifts. The higher drifts post-day 1105 are easily explained. Data sets with blank guide star drift fields (except day 978, an incomplete data set) were acquired using only one GS to control *HST* pitch and yaw. *HST* roll was controlled only by rate gyros. This operational mode results in generally poorer guiding, manifesting itself primarily as a monotonic drift in roll.

The group of higher drifts near day 814 may be due to several short-term effects. These include secondary mirror motions (the so-called mirror breathing) and possibly other thermal effects. As we shall see these short-term drifts are adequately handled by closure stars, no matter what the origin. However, the necessary inclusion of check stars in any *HST* astrometry adds time to the observation set, slightly decreasing the science acquired per unit time.

Our strategy for correcting the short-term instability, the drift seen in the check star (cf. Table 1 set 33) is a simple one. We assume that the drift rate is constant. Knowing the time between the first and last check star observations and the times of the observations in between, we apportion the drift accordingly, correcting each star position. The observation sets with statistically significant drift (bold in Table 1) have been corrected. We also corrected some of the larger drifts (>4 mas) which were seemingly not statistically significant. For most of these, the uncertainties in amount of drift were inflated by excessive jitter during the check star observation. We rely on the median to pull out a good centroid and apply a drift correction regardless.

To date we have identified only one long-term instability, changes in plate scale. This instability can be caused by either or both of the following two physical changes to *HST*. Any change in the distance between the primary and secondary mirrors of *HST* can cause a scale change. These two mirrors do change their separation because of desorption of the graphite-epoxy metering truss that holds them in relative placement (Hasan et al. 1993). This results in a change in magnification. Second, there may be components within an FGS whose orientations change from desorption or other causes. We have tentatively identified one of the lever arms (ρ_A, Bradley et al. 1991) as a possibly changing element within FGS 3.

Our method of correcting for long-term instabilities, primarily plate scale changes, includes both the present OFAD and a long-term stability monitoring (LTSTAB) test. For the results discussed below we include scale terms

in our model and adopt the scale in our present OFAD. For future astrometry we have instigated an observation series that will provide long-term monitoring of the scale. LTSTAB has become an integral component of OFAD maintenance, essential for tying present epoch observations to those acquired once an absolute *HST* scale has been determined at some time in the future.

LTSTAB monitors an ecliptic field, the star cluster M35. The field provides two unique and constant roll orientations. Since the *HST* solar arrays require normal incidence of sunlight, an ecliptic field can be observed all year with just two roll orientations. This is also the field observed to establish our OFAD. While at the antisun, very large off-nominal rolls of *HST* are permitted. Nearly 30 stars (including check stars) are observed at each of the two orientations. Our plan was to begin monitoring with one observation set per month. Due to the Sun constraint this would result in nine sets per year. The constant roll orientation allows tracking of OFAD changes, including scale. To date, various scheduling problems have not allowed us to obtain monthly checks. Hence, LTSTAB was not used to correct the OFAD for the data discussed in this paper. These data were reduced using the OFAD generated in January 1993.

Should LTSTAB detect only smooth and gradual changes, these trends could be removed with widely spaced monitoring of the check field. If the changes are smooth and rapid, more frequent monitoring will be necessary. If the changes are discontinuous, it may be necessary to observe the check field prior to each astrometry observation. The scale variations discussed in Sec. 3.3 will serve to determine the frequency of future LTSTAB observations.

Parallaxes and proper motions of the stars comprising our reference frame are a last possible systematic effect. However, the average magnitude of the reference frame is $V\sim 15$ (Table 2). Hence, the predicted parallactic and galactic rotation effects will be about half a millisecond of arc per year (van Altena 1993). We discuss the modeling of the proper-motion and parallax characteristics of our reference frame in Sec. 3.1.

3. ASTROMETRY

After correcting for systematic effects and throwing out the measures so affected by *HST* jitter as to be unsalvagable, our data consist of 299 star position measurements over the 40 observation sets. The x, y positions are obtained from medians. The positions have been corrected for a drift (if present) assumed to have a constant rate.

3.1 The Model

Except for details of the model [Eqs. (1) and (2) below], the analyses carried out here (using GAUSSFIT, Jefferys et al. 1988) are identical to those described in Benedict et al. 1991). The variances required by GAUSSFIT are provided by the jitter ball sizes. The overlapping plate method used here is described in Eichhorn and Jefferys (1971) and Jefferys (1979).

We solve for plate constants a, b, c, d, e, f and star parameters position (ξ and η), proper motion (μ), and parallax (π). We also determine R, the roll orientation of the constraint plate (which is observation set 6, obtained on day 757) with respect to right ascension and declination.

Our equations of condition for each observation set are

$$\xi = aX + bY + c - \mu_x t - [p_x \cos(R) - p_y \sin(R)]\pi, \quad (1)$$

$$\eta = dX + eY + f - \mu_y t - [p_x \sin(R) + p_y \cos(R)]\pi, \quad (2)$$

where the X, Y are positions of the stars in each observation set and p_x and p_y are parallax factors. The RA and DEC position for Proxima Cen (Benedict et al. 1992) was used in calculating p_x and p_y. The ξ and η are X, Y positions for the observation set chosen as our constraint, day 757. An Earth orbit predictor from JPL (DE200, Standish 1990) calculated the parallax factors.

Initially we constrained π and μ to zero for all stars, except Proxima Centauri, the check star. To search for planetary perturbations, we subject the position residuals of Proxima Cen to periodogram analysis (Press et al. 1992, Ch. 13.8). To identify any structure in the Proxima Cen periodogram possibly introduced by FGS 3 or *HST*, we inspect periodograms for each reference star. The periodogram for star 18 contained significant power at a period of one year. No other reference stars showed this. Hence, we solved for the proper motion and parallax of reference star 18 (see Sec. 3.4 below) relative to the remaining reference stars.

3.2 The Residuals

After determining plate constants and star parameters, each star in each observation set has an x and y residual, indicating how well the data fit the model. We present a broad overview of these residuals in Fig. 3. Histograms and gaussians fit to the histograms indicate that the distributions are reasonably gaussian and that our 1σ residual is 1.1 mas.

On the basis of these distributions, the 18 stars with residuals larger than ± 4 mas were branded as outliers. In some cases, the data were obviously affected by jitter, so much so that even a median filter gave a poor position. In other cases, no obvious defects in the data were found. We continue to interrogate *HST* engineering data for the underlying causes of such high residuals. We removed the outliers, representing 6.3% of our data, from the observation sets and obtained a new solution. For the rest of our discussion we consider only residuals from the solution that does not contain the outliers.

Rather than present a table containing the residuals for the remaining 263 stars, we derive the standard deviation for the x and y residuals for each star. This statistic offers an indication of the dispersion within a set of residuals. Similarly, the standard deviations for the x and y residuals for each observation set are calculated. Fig. 4 presents the standard deviations for each star and an RSS of the x and

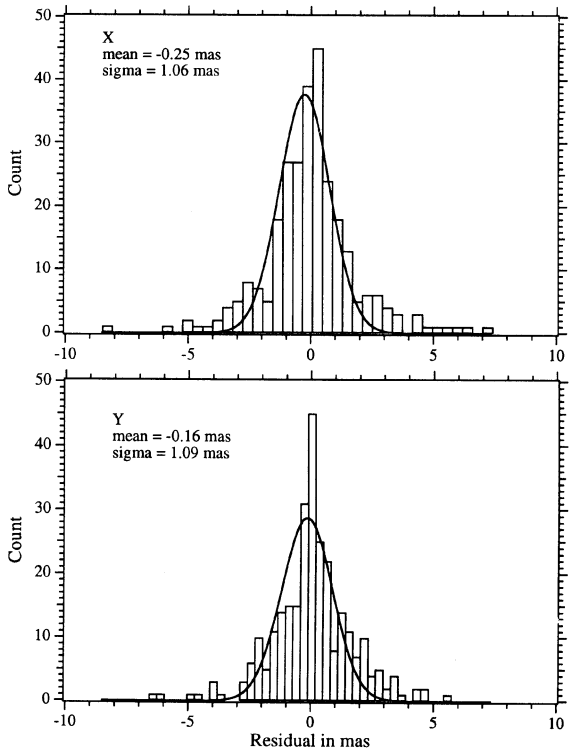

FIG. 3—Histograms of the residuals obtained by fitting 299 star positions contained in 40 observation sets to Eqs. (1) and (2). Residuals greater than 4 mas were declared outliers and removed from further consideration.

y standard deviation. Recall that stars 22 and 23 were only observed eight times, and at a single orientation. This single orientation probably drove the residuals down for these two stars. The average RSS standard deviation for all stars (omitting stars 22 and 23) is 1.9 mas.

In Fig. 5 we plot the *x* and *y* residual standard deviations as a function of observation date, e.g., for each observation set. We have previously noted the growth of the jitter balls, post day 859. There is no obvious discontinuity at day 859 in Fig. 5. However, the RSS residual standard deviations have grown from an average 1.8 mas to an average 2.2 mas pre- and post-day 859. We continue to get high quality centroids from these data, but the larger K_1 may be exacting a toll on our precision. Alternatively, some of the increase might be attributed to the increased drift in the data sets acquired with a single guiding FGS (Table 1, observation sets 32 and higher).

In Fig. 6, we plot the per star position residuals against stellar magnitude. In agreement with previous analyses (Benedict et al. 1992) the fainter stars have larger residuals. Finally, having discussed a possible color dependence, we display per star residual standard deviations against color index in Fig. 7 and find no systematic trends.

For either the entire pickle with fixed orientation or a field centered on and contained within the pickle center for all orientations, FGS 3 comfortably surpasses the prelaunch astrometric precision goal of 2.7 mas.

3.3 Scale Stability

The scale is the linear term in our OFAD (Jefferys et al. 1993). For this paper the absolute scale was determined by comparing our *HST* M35 observations with ground-based astrometry (McNamara and Sekiguchi 1986), upon which we impressed a scale from the ACRS (Corbin and Urban 1990). Since a full-up OFAD determination requires some 20 orbits, it is impractical to monitor scale changes with OFAD data. To provide an independent assessment of scale stability we use the Proxima Centauri field test data. We form a scale parameter

$$S = sqrt(ae - bd), \tag{3}$$

where unity scale is defined by observation set 6 (day 757). An S value less than unity for an observation set indicates that the field was larger, e.g., to bring the field back into coincidence with day 757, we must multiply by a number less than unity.

Figure 8 presents S vs. time. Typically, the more stars in the solution (NS, Table 1), the smaller the associated error in scale. The average $1-\sigma$ error in relative scale is 1.3×10^{-5}. We see a general trend upward, indicating a shrinking field.

There is one known change in primary–secondary separation. On day 858, the secondary was moved 14 μm away from the primary. This secondary mirror motion resulted in no statistically significant scale change. Thus, it is unlikely that the trend we see is due to primary–secondary mirror separation change, even though it is consistent with the sign of the scale change expected due to desorption of the graphite epoxy metering truss. It is likely that these scale-like variations are caused by some optical component within FGS 3 shifting due to graphite epoxy desorption.

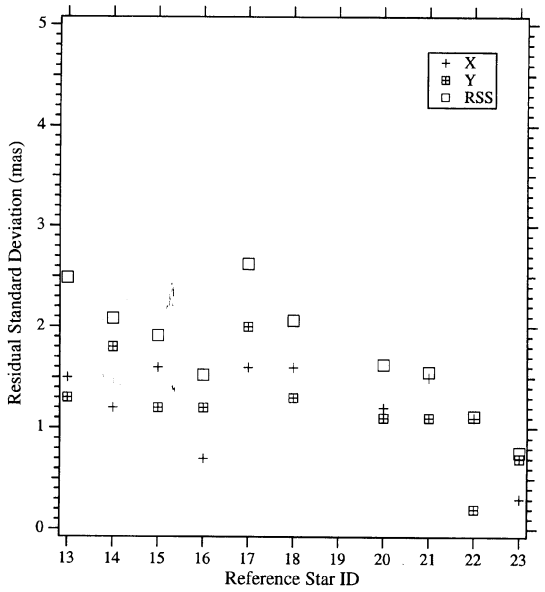

FIG. 4—Standard deviation of *x*, *y* position residuals and the RSS of *x* and *y* are plotted by star ID (Table 2). Star 22 and 23 were observed far fewer times and at only one orientation.

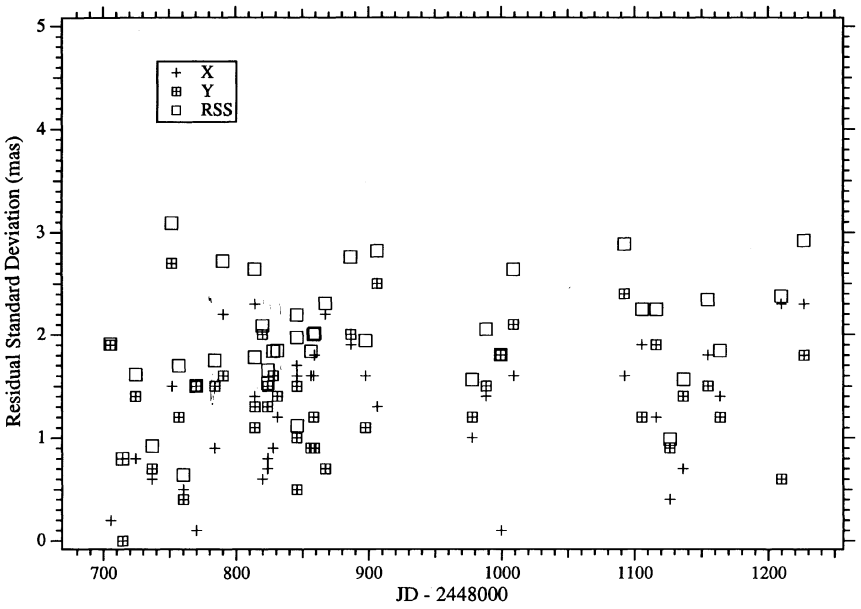

FIG. 5—Standard deviation of x, y position residuals and the RSS of x and y are plotted against date of observation. The interferometer gain values were increased on day 859. There is no obvious discontinuity, although the average standard deviation increased 0.5 mas. The gap centered on day 945 is solar avoidance. Guide star availability and scheduling time lag due to the temporary loss of FGS 2 guiding caused the gap centered at day 1050.

Are any of the short-term variations seen in Fig. 8 significant? Also plotted in Fig. 8 are the relative scales determined from two analyses of seven LTSTAB observation sets. For these analyses we remove proper motion and parallax from the model.

The first, second, and last LTSTAB sets were acquired with an identical FGS orientation. The remaining four were acquired with FGS 3 rolled 180°. The total number of stars in the overlap solution is 36. There are eight stars in the FGS 3 pickle center that are observed during both LTSTAB orientations. These eight stars provide the relative scale information between the two orientations. This analysis is labeled *LTSTAB FGS Center* in Fig. 8. The LTSTAB scale variations have been shifted arbitrarily in Y to force scale agreement near day 997. The average $1-\sigma$ error for these relative scale determinations is 8.8×10^{-6}.

The four points labeled *LTSTAB Spring* are from a scale solution using 29 stars over the entire FGS 3 pickle. These four observation sets had the identical orientation used in the Spring of 1993. The *Spring* point plotted farthest to the right consists of two observation sets taken one day apart. From this coincidence and from the average $1-\sigma$ error (2.5×10^{-6}) associated with the *Spring* scale determinations it is obvious that much of the observed scatter in scale is spurious or OFAD-induced. Scale errors at this level can introduce positional uncertainties of order 2 mas for two stars in the pickle separated by 15 arcmin.

The overall scale change trend is present in all solutions. Lastly, the Proxima observation set at day 978 has the

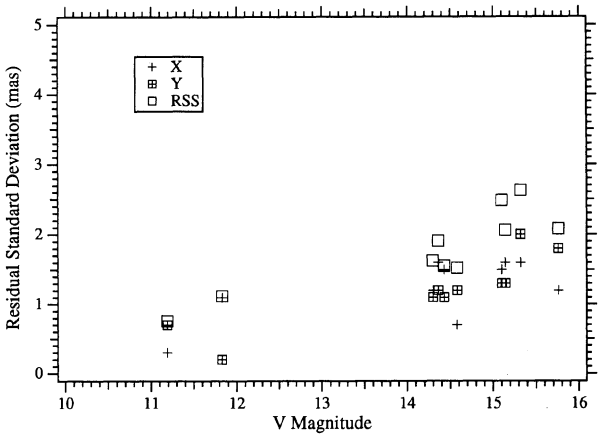

FIG. 6—The standard deviations of the position residuals show a slight (and expected) dependence on star magnitude.

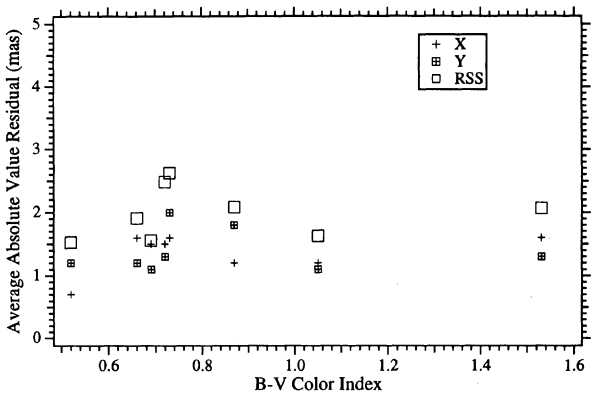

FIG. 7—The standard deviations of the position residuals show no dependence on star color. The expected lateral color effect seems small for this data set.

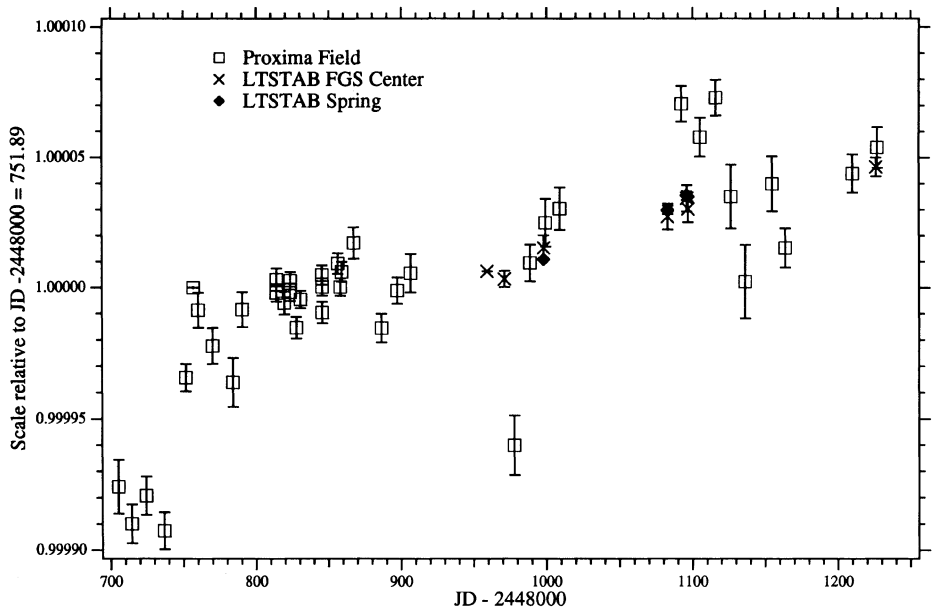

FIG. 8—Scale variations from the Proxima Cen field (□), LTSTAB center of pickle (×) and LTSTAB entire pickle Spring orientation (◆) as a function of observation data. Errors are $1-\sigma$.

smallest number of stars of any set and no drift check. *HST* jitter caused a loss of lock, halting the set prematurely. It is a suspect observation set. It is obvious from Fig. 8 that the Proxima field would not provide as precise a scale monitoring as does the LTSTAB M35 field.

The **quality** of the scale change is more important to *HST* FGS Astrometry than the **quantity** of change. We see few instances of significant scale change over times shorter than 30 days. It is evident from Fig. 8 that monthly LTSTAB observations will likely be required throughout the astrometric lifetime of *HST*. The scale changes seen will continue to be monitored, eventually understood, and removed. For now, the coefficients *a*, *b*, *d*, *e* [in Eqs. (1) and (2)] absorb scale variations. A decision to change the frequency of the LTSTAB observations can be made after we receive a relatively unbroken string of LTSTAB observation sets spanning 4 months.

3.4 The Parallax of Reference Star 18

We find for reference star 18 a relative parallax, $\pi_{\rm rel}=3.1\pm0.5$ mas. Reducing to absolute parallax based on the average brightness of the reference frame (van Altena 1993) we add 0.5 mas to obtain $\pi_{\rm abs}=3.6$ mas. Assuming a galactic reddening law $R=A_v/E(B-V)=3.1$ (Savage and Mathis 1979), the color and absolute magnitude are well matched by a G6 V star at a distance of 280 pc with $A_v=2.6$. This absorption, while high, is not unreasonable given the galactic longitude and latitude of the field ($l=316°$, $b=+2°$). Extinction is very patchy: areas within a degree show far less extinction, while near $l=318°$, $b=-2°$ Neckel and Klave (1980) see similar absorption. We find an absolute value proper motion $|\mu|=1.5\pm0.8$ mas y^{-1}, statistically indistinguishable from zero.

3.5 The 1 mas Catalog

Results of our plate solutions to Eqs. (1) and (2) include values for ξ and η with their associated errors. These are presented in Table 2. The average $1-\sigma$ errors for all stars are 1.2 and 1.5 mas in ξ and η. Excluding the edge stars (22 and 23 in Fig. 1) for which only one orientation and eight observation sets are available, we obtain average $1-\sigma$ errors of 0.7 and 0.9 mas in ξ and η.

This field may be useful as an astrometry check field to determine distortions at the 1 mas level. It cannot be used to determine absolute scale and rotation. We know neither the scale nor the transformation to RA and DEC with the precision of our ξ and η. Our ξ and η are in arcsec units, though the absolute scale has a small uncertainty (Sec. 3.3). We estimate systematic errors in star positions due to a lack of knowledge of the absolute scale to be of order 3 mas at the extremes of this 2.5 arcmin field.

In Table 2 we list the ξ and η and associated errors. As a convenience, we provide an RA, DEC produced by rotating the ξ and η from the day 757 orientation using $R=1.40703\pm0.00058$ rad. This R resulted from the solution of Eqs. (1) and (2). Taking the position of star 15 from Benedict et al. (1993), we calculate RA and DEC from the relative offsets given by the rotated ξ and η. The absolute position of Star 15, and thus, the entire catalog, is known to only ±80 mas.

We did not achieve a root N reduction in the position errors. If a single observation gives 2 mas, 40 observations should give ~0.3 mas. We achieve about 1 mas. The OFAD is the likely cause of this. We cannot do any better than the OFAD mapping, which breaks down (Jefferys et al. 1994) at the 1 mas level of precision.

3.6 Precision for A One-Year Subset

Observing time on *HST* is a scarce and carefully allocated resource. Few projects in astrometry are likely to obtain the volume of data discussed in this paper. Consequently, it becomes useful to ask what precision could be attained with the number of data sets likely to be granted a typical astrometry enterprise, during a single 12-month period. To answer this question, we repeat the reductions on a subset of the data consisting of sets 1, 6, 10, 13, 19, 24, 26, 29, 31, and 32 (Table 1). These data cover a time duration of 387 days and include several gaps. The edge stars (22 and 23 in Fig. 1) were excluded for these solutions. These dates were not chosen to maximize parallax factors.

For reference star 18 we find a relative parallax, $\pi_{\rm rel}=3.1\pm1.0$ mas. We determine an absolute value proper motion $|\mu|=1.6\pm2.2$ mas y^{-1}. For the reference star catalog we obtain average $1-\sigma$ errors of 1.0 and 1.2 mas in ξ and η. Relative positions and parallaxes comparable to ground-based techniques applied over 3–6 years (e.g., Monet et al. 1992) can be secured for roughly 4 hr of on-target time over one year. Longer time spans are required for precise proper motions.

4. CONCLUSIONS

The center of FGS 3 produces very high precision astrometry. Per observation RSS positions with 2.0 mas precision are obtainable down to $V=15.8$. Distances good to 20% can be obtained for stars as faint as $V=15$ at $d=300$ pc. We present a catalog containing eight stars within a 2.5-arcmin circle whose relative positions have errors of order 1 mas, excluding a systematic scale contribution.

There are gradual changes that manifest as scalelike. It is possible that these scalelike variations are caused by some optical component within FGS 3 shifting due to graphite epoxy desorption. Future monitoring with LTSTAB will likely maintain the relative scale to better than 2.5 parts in 10^6. The frequency of monitoring will probably remain in the range six to nine times per year.

We continue to refine the data reduction, adding corrections to the data and/or new reduction techniques as our understanding of systematic errors increases. Each refinement has improved our astrometry. We have several corrections not yet implemented. The precision of *HST* POS mode astrometry will likely further improve.

Successful FGS POS mode astrometry depended on the efforts of many. At the Space Telescope Science Institute, we thank John Hershey, Glenn Schneider, Chris Blades, Denise Taylor, Lauretta Nagel, Brett Blacker, and Shireen Gonzaga for commanding, proposal and scheduling assistance, and Mario Lattanzi and Larry Taff for critical review and corroboration of early results. Dave Leckrone and Keith Kalinowski at Goddard Spaceflight Center provided essential counsel and representation. Linda Abramowicz-Reed and Christ Ftaclas at Hughes–Danbury Optical Systems provided FGS engineering insight. Art Bradley of Allied Signal Aerospace Company managed several key pointing control system improvements. We thank the referee, Dave Monet, for suggestions improving the quality of this paper. This work was supported by NASA Contract NAS5-29285 and NASA Grant NAG5-1603.

REFERENCES

Abramowicz-Reed, L. 1993, private communication
Benedict, G. F., McGraw, J. T., Hess, T. R., Cawson, G. M., and Keane, M. J. 1991, AJ, 101, 279
Benedict, G. F., Nelan, E., Story, D., McArthur, B., Whipple, A. L., Jefferys, W. H., van Altena, Wm. F., Hemenway, P. D., Shelus, P. J., McCartney, J. E., Franz, O. G., Fredrick, L. W., Bradley, A., and Duncombe, R. L. 1992, PASP, 104, 958
Benedict, G. F., Nelan, E., McArthur, B., Story, D., Whipple, A. L., Jefferys, W. H., van Altena, Wm. F., Hemenway, P. D., Shelus, P. J., McCartney, J. E., Franz, O. G., Fredrick, L. W., Bradley, A., and Duncombe, R. L. 1993, PASP, 105, 487
Bradley, A., Abramowicz-Reed, L., Story, D., Benedict, G., and Jefferys, W. 1991, PASP, 103, 317
Bahcall, J. N., and O'Dell, C. R. 1979, in Scientific Research with the Space Telescope, IAU Coll. 54, NASA CP-2111
Corbin, T. E., and Urban S. E. 1990, in Inertial Coordinate System on the Sky, ed. J. Lieske and V. Abalakin (Dordrecht, Kluwer), p. 433
Eichhorn, H., and Jefferys, W. H. 1971, Proceedings of the Fourth Astrometric Conf., ed. P. A. Ianna (Leander McCormick Obs. 16, 267)
Ftaclas, C. 1993, private communication
Hasan, H., Burrows, C. J., and Schroeder, D. J. 1993, PASP, 105, 1184
Jefferys, W. H. 1979, AJ, 84, 1775
Jefferys, W. H., Benedict, G. F., Hemenway, P. D., Shelus, P. J., and Duncombe, R. L. 1985, Celest. Mech., 37, 3, 299
Jefferys, W. H., Fitzpatrick, M. J., and McArthur, B. E. 1988, Celest. Mech., 41, 39
Jefferys, W. H., Whipple, A. L., Wang, Q., McArthur, B., Benedict, G. F., Nelan, E., and Story, D. 1994, Proceedings of HST Calibration Workshop, Nov. 1993
McNamara, B., and Sekiguchi, K. 1986, AJ, 91, 557
Monet, D. G., Dahn, C. C., Vrba, F. J., Harris, H. C., Pier, J. R., Luginbuhl, C. B., and Ables, H. D. 1992, AJ, 103, 638
Neckel, T., and Klave, G. 1980, A&AS., 42, 251
Press, W. H., Teukolsky, S. A., Vetterling, W. T., and Flannery, B. P. 1992, Numerical Recipes in Fortran, Second Edition (Cambridge, Cambridge University Press)
Savage, B., and Mathis, J. 1979, ARAA, 17, 73
Standish, E. M. 1990, A&A, 233, 252
van Altena, Wm. F. 1993, private communication
Wissenger, A., and Carricato, R. 1976 in The Space Telescope, NASA SP-392